

Laser desorption/ionization MS imaging of cancer kidney tissue on silver nanoparticle-enhanced target

Adrian Arendowski^{*1}, Joanna Nizioł¹, Krzysztof Ossoliński², Anna Ossolińska², Tadeusz Ossoliński², Zygmunt Dobrowolski² & Tomasz Ruman¹

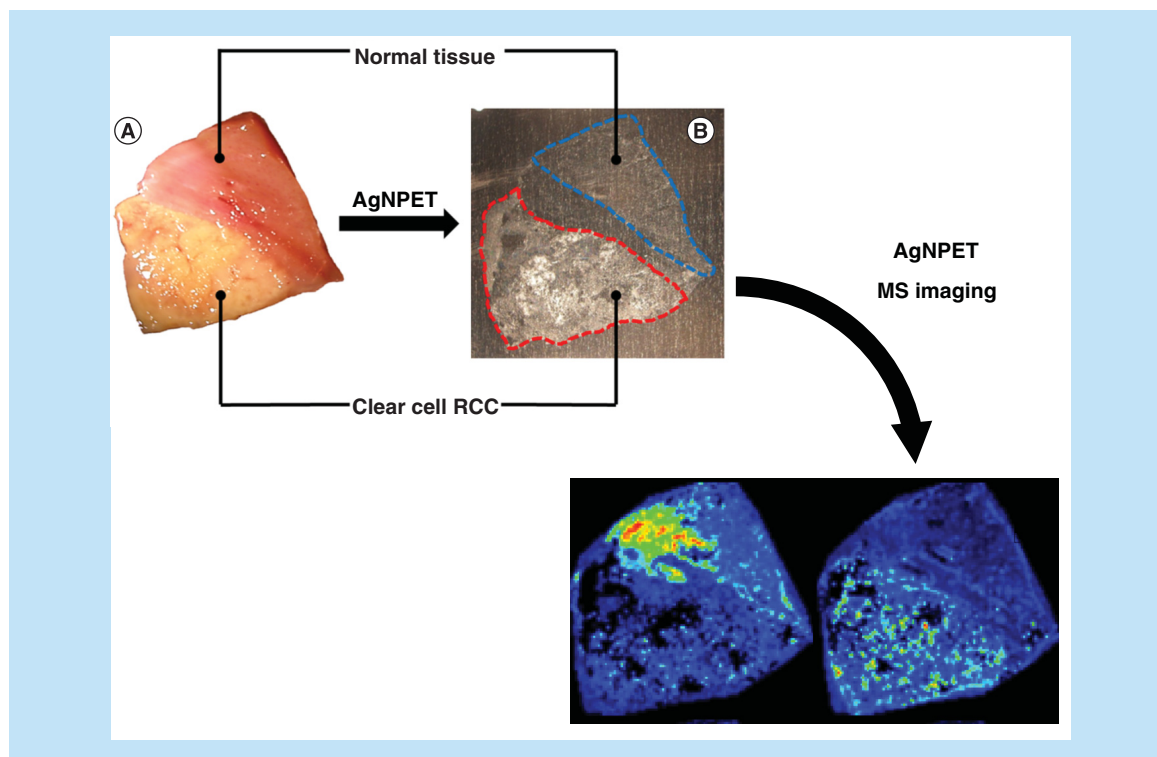
¹Faculty of Chemistry, Rzeszów University of Technology, 6 Powstańców Warszawy Ave, 35-959, Rzeszów, Poland

²Department of General Surgery & Urology, John Paul II Hospital, Grunwaldzka 4 St, 36-100, Kolbuszowa, Poland

* Author for correspondence: Tel.: +48 17 743 2012, adrian@arendowski.hub.pl

Aim: Renal cell carcinoma is a very aggressive and often fatal disease for which there are no specific biomarkers found to date. The purpose of work was to find substances that differentiate the cancerous and healthy tissue by using laser desorption/ionization MS imaging combined with silver nanoparticle-enhanced target. **Results:** Ion images and comparative analysis of spectra revealed differences in intensities for several metabolites, for which their biochemical properties were discussed. Statistical analysis allowed to distinguish healthy and cancer tissue without the involvement of a pathologist. **Conclusion:** Laser desorption/ionization MS imaging technology combined with silver nanoparticle-enhanced target enabled rapid visualization of the differences between the clear cell renal cell carcinoma and the healthy part of the kidney tissue.

Graphical abstract:



First draft submitted: 6 September 2017; Accepted for publication: 23 October 2017; Published online: 14 December 2017

newlands
press

Keywords: kidney cancer • laser desorption/ionization • MS imaging • renal cell carcinoma • silver nanoparticles

According to GLOBOCAN, in 2012, there were approximately 338,000 new cases of kidney cancer and 144,000 deaths due to this disease [1]. More than 80% of adult kidney cancers are renal cell carcinomas (RCCs) [2]. RCCs are heterogeneous group of cancers divided into several subtypes: clear cell (80% of cases), papillary (10%), chromophobe (5%), medullary and collecting duct (below 1%) and other unclassified subtypes (~5%) according to WHO classification [3]. These tumor subtypes differ from each other on morphological and genetic levels as well as have a different prognoses [3]. About 30% of patients have metastases at the time of diagnosis which significantly worsens the prognoses. This is due to the fact that most of the time RCC develops asymptotically and is often diagnosed in advanced stages, usually by incidental radiologic examination [4]. Thus, RCC still remains a major challenge and forces searching for early detection procedures, for example, the ones based on the detection of cancer biomarkers distinctive chemical compounds that might indicate a development of tumor.

Diagnostic markers can be genes [5], proteins [6] and metabolites [7], but proteomic approach predominates in current strategies of cancer biomarker search. The mostly used family of methods in cancer biomarker research is MS. Among the various techniques of ionization, MALDI technique deserves special attention. Due to the soft ionization, very high sensitivity over a wide mass range and high mass determination accuracy, this technique is among the best choices for biomaterial analysis. MALDI has already been used as a tool for cancer diagnostics [8,9] including RCC protein and peptide profiling [10].

MALDI MS experiments may be performed also in imaging mode which preserves information about spatial distribution of substances in object. MS imaging (MSI) makes correlation of ion images with histological features of tissue possible [11], allows analysis of the distribution of chemical compounds in cancerous and normal tissue and thus helps discovering of new candidates for biomarkers [9].

MALDI MSI of RCC has repeatedly been used by researchers [12–16]. However, conventional approach with commonly used low-molecular-weight organic acids as matrices possesses limitations such as: high chemical background in the low mass region (up to m/z 800), low mass determination accuracy due to large thickness of measured object and sweet-spot effect. Another important disadvantage is the application of commonly used external calibration, which is inferior to internal one. What is more, acidity of matrix solution is problematic for analysis of acid-labile biological compounds. Complicated sample preparation is a handicap of MALDI MSI as procedure involves several steps such as freezing and cutting of the tissue into thin slices, defrosting, deposition of tissue on the target plate and application of matrix layer [17]. These problems make MALDI not a best choice for the identification, analysis and imaging of low-molecular-weight compounds, and thus for low-molecular-weight biomarker research.

Most of above mentioned problems may be avoided by application of different types of matrix-less methods such as surface-assisted laser desorption/ionization (LDI) [18] family of laser-based MS methods. Recent article of our group describes the application of surface-transfer technique for analysis of kidney tissue on gold nanoparticle-enhanced target [19]. Results of MSI allowed to propose two low-molecular-weight compounds – octadecanamide and diglyceride (DG; 18:1/20:0) as potential biomarkers of RCC. Examined samples in the mentioned study [19] were collected from 80-year-old patient with diagnosed clear cell renal cell carcinoma (ccRCC) Fuhrman grade III and invasion into renal capsule. Comorbidities included: diabetes Type II, hypertension and hyperthyroidism.

In this study, we analyzed specimens from patient diagnosed with renal tumor who underwent radical nephrectomy. MS analysis of tissue from healthy renal region was compared with cancerous tissue with pathologically confirmed ccRCC Fuhrman grade IV, invasion into perinephric adipose fat and lymph node and distant metastases.

Silver ions produced from silver nanoparticles in laser irradiation process have different ionic radii and electron affinity compared with gold ones and thus different cationization efficiency for given analyte. Furthermore, it was suggested by some authors that silver nanoparticles have higher affinity for low polarity compounds. For above mentioned reasons, application of AgNPs for detection of potential biomarkers can provide different results compared with nanoparticles of other metals. Successful application of gold nanoparticles for MSI of RCC tissue [19] suggests that silver nanoparticles, which due to their absorption characteristics are highly beneficial for ultraviolet laser-based MS [20], should provide interesting insight into chemistry and biochemistry of ccRCC. For these reasons, our silver nanoparticle-enhanced target (AgNPET) [21] was chosen for this work.

Experimental

Cancer tissue

Research protocol was approved by the local bioethics committee at the University of Rzeszów (Poland). Patient who agreed to participate in the study, donated 10 ml of blood, 50 ml of urine and approximately 1 cm³ of cancerous tissue containing small margin of normal tissue. Tissue was removed *ex vivo* after surgical resection of kidney. The specimen described in this work was obtained from a 59-year-old man. Computed tomography scan revealed the presence of 7.5 cm tumor without metastasis to lymph node or other organs. Histopathological examination confirmed that analyzed tissue is RCC, subtype: clear cell, Fuhrman IV with 10% necrosis within tumor and invasion into fibrous capsule and perinephric adipose tissue.

Materials & methods

Silver trifluoroacetate used in nanoparticle synthesis was of 99.99+% purity (Sigma-Aldrich, MO, USA). 2,5-Dihydroxybenzoic acid was purchased from Bruker Daltonics GmbH (Bremen, Germany). All other chemicals were purchased from Sigma-Aldrich, Poznań, Poland (97–99% purity). All solvents were of HPLC quality. AgNPET plate was prepared according to the protocol described previously [21] from mirror-finish plate of magnetic stainless steel of H17 grade (locally made) and used with Bruker NALDI[®] adapter. Optical photographs were made with the use of an Olympus SZ61TR microscope equipped with an 8 MPix Olympus digital camera.

Sample preparation & MSI experiment

Tissue sample as obtained after surgery was immediately frozen and stored at -24°C. Unfreezing step was performed in room temperature. Flat tissue surface selected for imaging was gently and uniformly pushed against few-millimeter thick stack of pure-cellulose filter papers for collection of liquid material with frequent changing of paper stack. After unfreezing, tissue surface was then touched to AgNPET plate allowing the two surfaces to contact each other for a few seconds, after which the sample was removed and the target surface was air dried and inserted into MS apparatus.

Measurements were performed with a Bruker Autoflex Speed time-of-flight mass spectrometer in positive-ion reflectron mode. The instrument was equipped with a solid state laser – SmartBeam II 1000 Hz, 355 nm (Bruker Daltonics GmbH, Bremen, Germany). Laser impulse energy was approximately 100–190 µJ and laser pulse repetition rate was 1 kHz. The imaging experiment was made at 200 µm × 200 µm resolution with 500 laser shots per individual spot and with a default random walk applied (FlexImaging 4.0 [Bruker Daltonics GmbH]). Spectra were recorded in the *m/z* range of 200–1400, with ions below *m/z* 190 deflected from the flight trajectory. In reflectron mode, the operating conditions voltages were as follows: ion source 1, 19 kV; ion source 2, 16.7 kV; lens 8.4 kV; reflector 1, 21 kV; reflector 2, 9.55 kV. The delay time was 150 ns. Spectra were calibrated on 14 points using internal standards (silver ions and clusters from Ag₂⁺ to Ag₉⁺). All of the shown imaging pictures were for ± 0.05% *m/z* window and total ion current (TIC) normalization was used throughout.

Analysis of the results

The average spectra of the imprint area of healthy and cancerous tissue were generated and then compared in the program SCiLS Lab v2016 b. Ion images and statistical analysis were performed using the Cardinal (R package) [22] with hotspot suppression and Gaussian smoothing applied. Database search of chemical compounds were carried out using a custom made program. Calculated and experimental *m/z* differences for all identified compounds are below 10 p.p.m., *m/z* values were calculated using the program ChemCalc available online [23].

Results & discussion

AgNPET MSI of kidney tissue

The aim of the research was to investigate the applicability of LDI MSI with the use of silver nanoparticle-enhanced surface-assisted LDI-type target AgNPET to the analysis of human tissue, and in particular, to kidney cancer biomarker research. Renal tissue with prominent area occupied by the cancer (Figure 1A) was obtained as a result of surgical removal, and then processed as described in the 'Experimental' section. Imprint of an object on AgNPET was imaged with a spatial resolution of 200 µm × 200 µm, which allowed to obtain total amount of 7972 mass spectra. Out of large amount of generated ion images, ten were selected as the most differentiating between healthy and cancerous areas and these are shown in Figure 1C–L and are listed in Table 1.

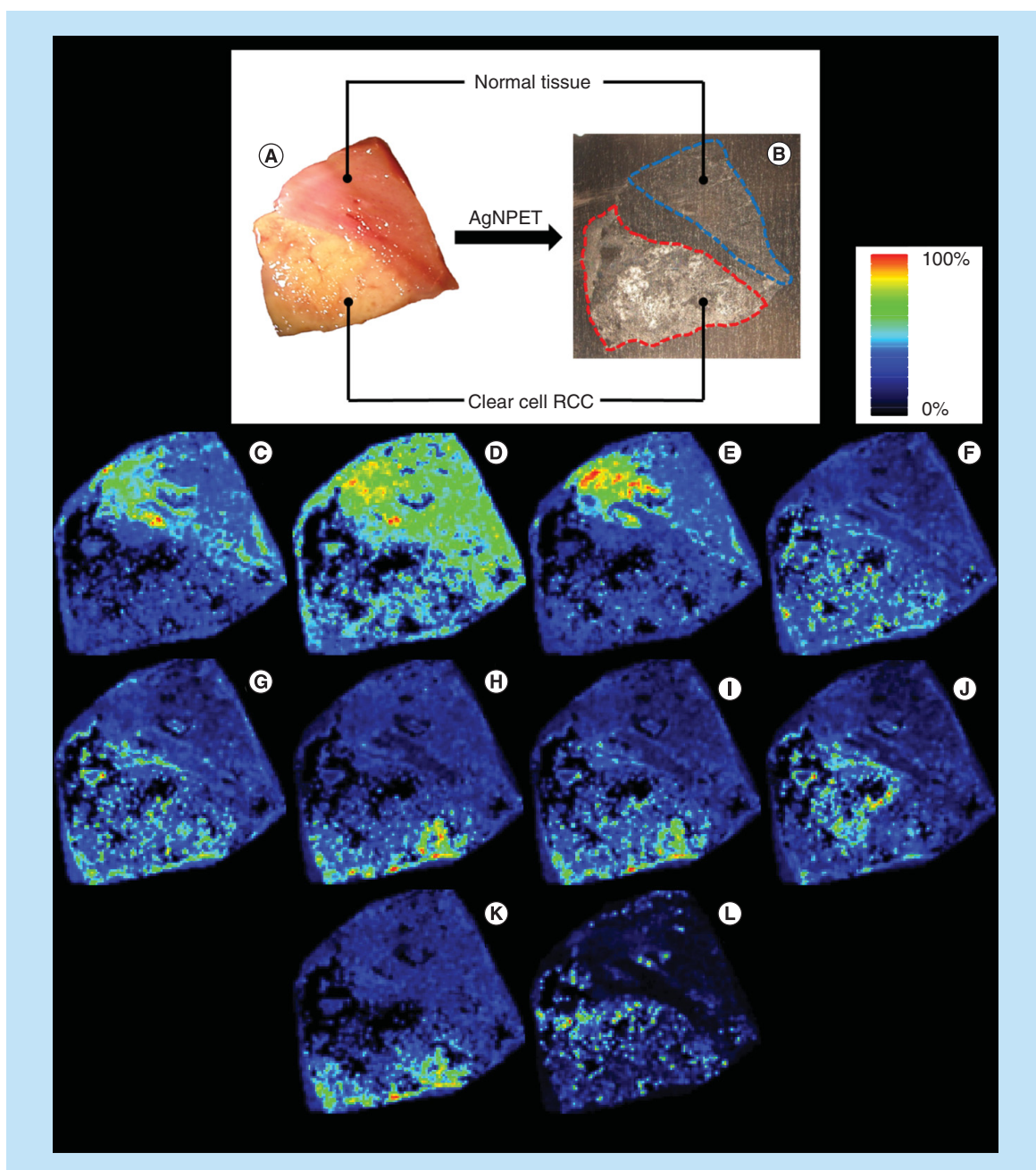


Figure 1. Results of MS imaging. Optical photograph of the imaged surface of the kidney specimen (A) and its imprint on the AgNPET plate (B). Images (C–L) contain ion images for m/z values of 203.053 (C), 232.037 (D), 286.968 (E), 389.132 (F), 392.192 (G), 411.145 (H), 415.101 (I), 417.191 (J), 437.100 (K) and 538.483 (L), respectively. Spatial resolution of ion images is $200\ \mu\text{m} \times 200\ \mu\text{m}$. AgNPET: Silver nanoparticle-enhanced target.

Three adducts of m/z values of 203.053 (Figure 1C), 232.037 (Figure 1D) and 286.968 (Figure 1E) show higher intensity within healthy tissue as judged from generated ion images, and the next seven adducts (Figure 1F–L) are characterized by a higher intensity in the tumor tissue.

Two of the ion images show the spatial distribution of the compound of formula $\text{C}_6\text{H}_{12}\text{O}_6$, one of them represents ion image of the sodium (Figure 1C) and the other one of the silver-107 adduct (Figure 1E). Human metabolome database (HMDB) contains only four records of compounds of the mentioned molecular formula that were detected and quantified in kidneys. Three of them are monosaccharides – glucose, sorbose and mannose

Table 1. Laser desorption/ionization MS imaging analysis results of kidney tissue imprint on silver nanoparticle-enhanced target.

Compound name	Ion formula	m/z [†]	Image
Glucose	[C ₆ H ₁₂ O ₆ +Na] ⁺	203.053	Figure 1C
Glucose	[C ₆ H ₁₂ O ₆ +Ag ¹⁰⁷] ⁺	286.968	Figure 1E
Phenylacetylglycine	[C ₁₀ H ₁₁ NO ₃ +K] ⁺	232.037	Figure 1D
Sulfapyrazone sulfide	[C ₂₃ H ₂₀ N ₂ O ₂ S+H] ⁺	389.132	Figure 1F
Octadecanamide	[C ₁₈ H ₃₇ NO+Ag ¹⁰⁹] ⁺	392.192	Figure 1G
Arachidonic acid	[C ₂₀ H ₃₂ O ₂ +Ag ¹⁰⁷] ⁺	411.145	Figure 1H
Riboflavin	[C ₁₇ H ₂₀ N ₄ O ₆ +K] ⁺	415.101	Figure 1I
Eicosenoic acid	[C ₂₀ H ₃₈ O ₂ +Ag ¹⁰⁷] ⁺	417.192	Figure 1J
S-Adenosyl-L-methionine	[C ₁₅ H ₂₂ N ₆ O ₅ S+K] ⁺	437.100	Figure 1K
N-(2-hydroxypentadecanoyl)-4,8-sphingadine	[C ₃₃ H ₆₃ NO ₄ +H] ⁺	538.483	Figure 1L

[†] Calculated m/z for ion in second column.

– and the other one is formally an oligohydroxylic alcohol myoinositol. As HMDB suggests, glucose occurs in blood in 50–200 higher concentration compared with three other listed compounds, which strongly suggests that both ion images (Figure 1C & E) present distribution for glucose ions. In case of our results, MSI suggests that higher concentration of glucose is in the normal tissue region as judged by distribution of glucose–sodium and glucose–silver adducts. This result is in contrast with results of derivatization-applied GC time-of-flight MS analysis presented by Catchpole *et al.* [24], who have shown that glucose were found in higher concentrations in cancer tissue compared with normal one. However, other researchers have found much lower glucose concentrations in both colon and stomach tumor tissues. Mentioned levels of glucose in normal and tumor colon tissues were 1220 ± 150 (mean \pm SE) and 123 ± 43 nmol/g, respectively. Levels for stomach tissues were 1290 ± 168 and 424 ± 131 nmol/g for normal and cancer ones, respectively [25]. It seems rational to expect lower glucose concentrations in cancer tissue as this result indicate enhanced glycolysis and thus confirm the Warburg effect [26]. The latter effect states that most cancer cells are exposed to chronic hypoxia from the early stage of carcinogenesis, which results in predominant use of glycolysis rather than oxidative phosphorylation for energy production, regardless of availability of oxygen.

Another ion picture that shows higher intensity in the area of healthy tissue has been created for the mass 232.037 Da, which corresponds to the potassium cation adduct of C₁₀H₁₁NO₃ formula (Figure 1D). Compounds assigned to this peak were previously considered as potential biomarkers for kidney cancer, and these are phenylacetylglycine [27] and methylhippuric acid [28], both chemical compounds are acyl derivatives of glycine. What is interesting, phenylacetylglycine was previously classified as a presumed surrogate marker of phospholipidosis [29].

An interesting ion image was generated for mass 392.192 (Figure 1G), which was assigned to the octadecanamide adduct with silver-109 isotope. Octadecanamide is a fatty amide of stearic acid and is a common metabolite associated with the pathway of fatty acid metabolism. The protonated ion of this chemical compound was also found in cancer region of renal tissue in our recent work [19], in which a different gold nanoparticle-based method was used. Interestingly, ions of this compound were found in higher intensities in the cancer region of both studied specimens, which confirms our earlier proposals [19] of considering this compound as a ccRCC tissue biomarker.

Figure 1H contains ion image of ion assigned to silver-107 adduct of arachidonic acid. This ion was found to be in higher intensity in the cancer region of kidney tissue. Arachidonic acid is a polyunsaturated fatty acid occurring in animals. Published data showed that the arachidonic acid level in RCC tissue was lower than that of normal kidney tissue, but higher levels were found in metastasized tumors [24]. Arachidonic acid has pro-inflammatory properties and is a substrate for cyclooxygenase or lipoxygenase pathway which generates eicosanoids that are associated with the pathogenesis of many diseases, including cancer. Increased expression of cyclooxygenase and lipoxygenase has also been demonstrated for renal tumor [30]. Production of eicosanoids is a complex process initiated by the release of arachidonic acid from cellular lipids by phospholipase A2, whose activity and expression is increased in several types of human tumors [31], this may in some way explain the elevated level of arachidonic acid in the tumor tissue relative to the healthy one.

Chemical compound for which ion image Figure 1I was generated and for which the area of higher intensity coincides with the cancer region is riboflavin (vitamin B2). It is an important biochemical element necessary for the proper functioning of the human organism, because riboflavin and related compounds are essential requirements for cell growth and development. Vitamin B2, is the precursor of the coenzymes, which are involved in energy production as crucial for the metabolism of carbohydrates, proteins and fats [32]. Literature does not contain any information regarding its levels in healthy and cancer tissue; however, some authors suggested that at higher concentrations riboflavin enhances cancer cell proliferation [33], others suggested antitumor activity [34].

Another image showing a higher intensity within the RCC was created for the ion of formula $[C_{20}H_{38}O_2+Ag^{107}]^+$ (Figure 1J), which was assigned to eicosenoic acid, which had previously been found in kidney tissue [19]. This substance is a monounsaturated omega-9 fatty acid occurring in both animals and plants.

Ion image shown in Figure 1K presents spatial distribution of ion of m/z 437.100 Da, which corresponds with potassium adduct of *S*-adenosyl-L-methionine (SAM). This compound is an important molecule synthesized in the cytosol of every living cell. SAM plays role in three metabolic pathways: transsulfuration, transmethylation and polyamine synthesis and is a key compound essential for proper cell function and survival. The tremendous role of methylation in many cellular mechanisms such as gene expression and membrane fluidity, as well as the necessity of polyamines for cell growth, make changes in SAM level likely to affect cell function and development [35]. On the basis of MSI, it can be seen that the higher intensity of SAM is in the RCC region. This metabolite has not yet been considered as a potential biomarker of renal tumor, but most probably it is involved in hepatocarcinogenesis [36]. The last of the presented ion images was generated for value 538.483 m/z (Figure 1L). It was assigned to ion of the formula $[C_{33}H_{63}NO_4+H]^+$, which is the proton adduct of the *N*-(2-hydroxypentadecanoyl)-4,8-sphingadienine. It is a ceramide that has not been reported in literature as a potential biomarker until now.

Cancer-normal tissue differentiation with statistical analysis

In order to check whether normal renal tissue can be distinguished from cancer one, principal component analysis (PCA) and spatial segmentation (k-means clustering) statistical methods implemented in Cardinal package were used. PCA is a multidimensional statistical technique commonly used for analyzing MSI data. This method helps revealing the spatial structures contained in a dataset, by grouping variables with high covariance [37]. The graphical results of calculation of first six PCA components are shown in Figure 2A–F, while PCA plots are included in Supplementary Material 1. Basically, images of first four calculated components allow differentiation of cancer region from the rest of the tissue surface as the most intense signals are almost exclusively in cancer region. However, it is desired that automated analysis method should produce colored areas including whole cancer and/or normal tissue regions allowing fast differentiation between tissue types.

The second method of statistical analysis used was k-means spatial segmentation [38] available in Cardinal. The calculation results generated for the parameters defined as the neighborhood smoothing radius $r = 5$ and the number of clusters/segments $k = 2, 5, 10$ and 15 are shown in Figure 2G–J. Spatial segmentation summary and mean spectra are available in Supplementary Material 2. The spatial segmentation images (Figure 2G–J) suggest that the greater part of the tumor-altered tissue fragment was grouped into one cluster and is distinguishable from the remaining area (Figure 2G). There are also some artifacts in the normal kidney tissue area, which may be due to the hidden structures of this tissue. It is also possible that pathological state begins to develop in this area. Further clustering has revealed more groups that were located mostly in the cancer region of the imprint area (Figure 2H & I). What is interesting, the use of 15 segments allowed to completely differentiate the entire imprint from the background (Figure 2J).

Analysis of differences in average MS spectra

Data derived from MSI experiment was additionally analyzed by comparison of average spectra of cancer and normal areas (Figure 3) which allowed for the creation of a list of peaks with distinctly different intensities.

Comparative analysis of average MS spectra of cancer and normal regions allowed to find 25 m/z values for which the ratio of absolute intensities was higher than 2 or lower than 0.5. Three of them were found in the normal tissue area and 22 m/z values were of higher intensities in the cancer tissue area. Average spectra fragments generated in SCiLS program for these differentiating signals for cancer and normal areas are shown in Supplementary Material 3 & 4. Identification on the basis of m/z value and also isotopic pattern yielded data presented in Table 2. It should be noted that all three of them are having characteristic isotopic patterns typical for natural silver-107 and silver-109 adducts.

Table 2. List of ions and compounds found by comparison of average spectra.

Compound name	Ion formula	Ratio of intensity parameters [†]	Experimental m/z	Calculated m/z	Δ m/z (p.p.m.)
Squalene	$[C_{30}H_{50}+^{107}Ag]^+$	0.48	517.298	517.2958	4.3
Palmitoyl glucuronide	$[C_{22}H_{42}O_7+^{107}Ag]^+$	0.41	525.202	525.1976	8.4
<i>N</i> -stearoyl arginine	$[C_{23}H_{46}N_4O_3+^{107}Ag]^+$	0.38	533.262	533.2615	0.9

[†]Ratio of intensity parameters was calculated by dividing absolute intensity in cancer tissue by the same parameter of normal tissue. Absolute intensity parameter of average spectra was read directly from SCILS program.

An ion found at m/z value of 517.298 was assigned to the silver-107 adduct of $C_{30}H_{50}$ formula. There are 12 compounds of the same formula in the metabolic databases, but among them, squalene was the only one recorded in the HMDB. Squalene is polyunsaturated hydrocarbon occurring naturally in living organisms. It is a metabolic precursor of sterols, including cholesterol, steroid hormones and vitamin D. It was shown that kidneys are one of the organs involved in the synthesis of squalene [39]. It is believed that squalene molecules may play a role in inhibiting tumor growth [40]. This could partially explain its higher content in normal renal tissue compared with

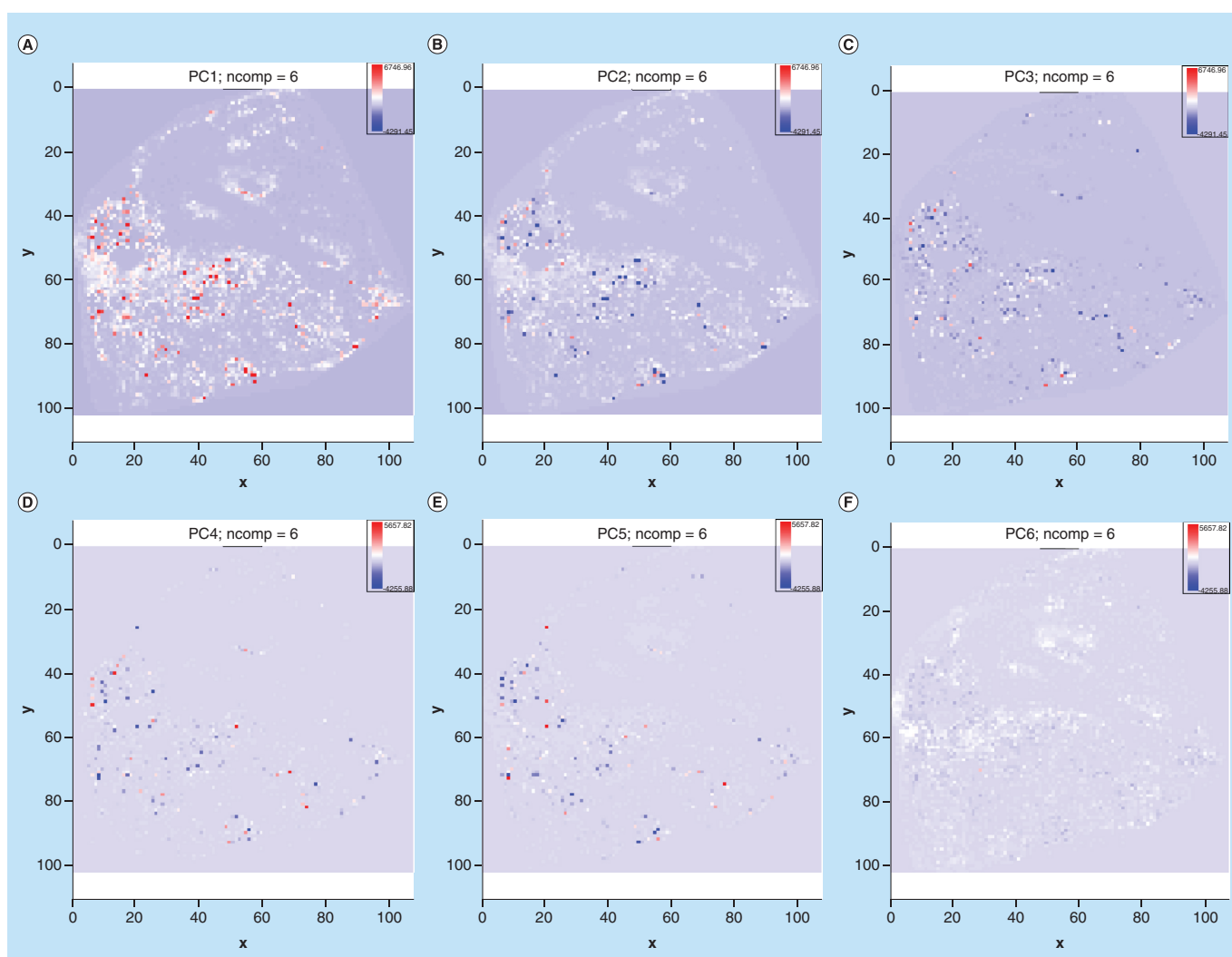


Figure 2. Statistical analysis of MS imaging results. Graphical representations of spatial distributions for six PCA components generated in Cardinal (A–F) and images of Gaussian k-means clustering of studied imaging data generated with following parameters: smoothing radius $r = 5$, number of segments $k = 2$ (G); $k = 5$ (H); $k = 10$ (I); $k = 15$ (J). PCA: Principal component analysis.

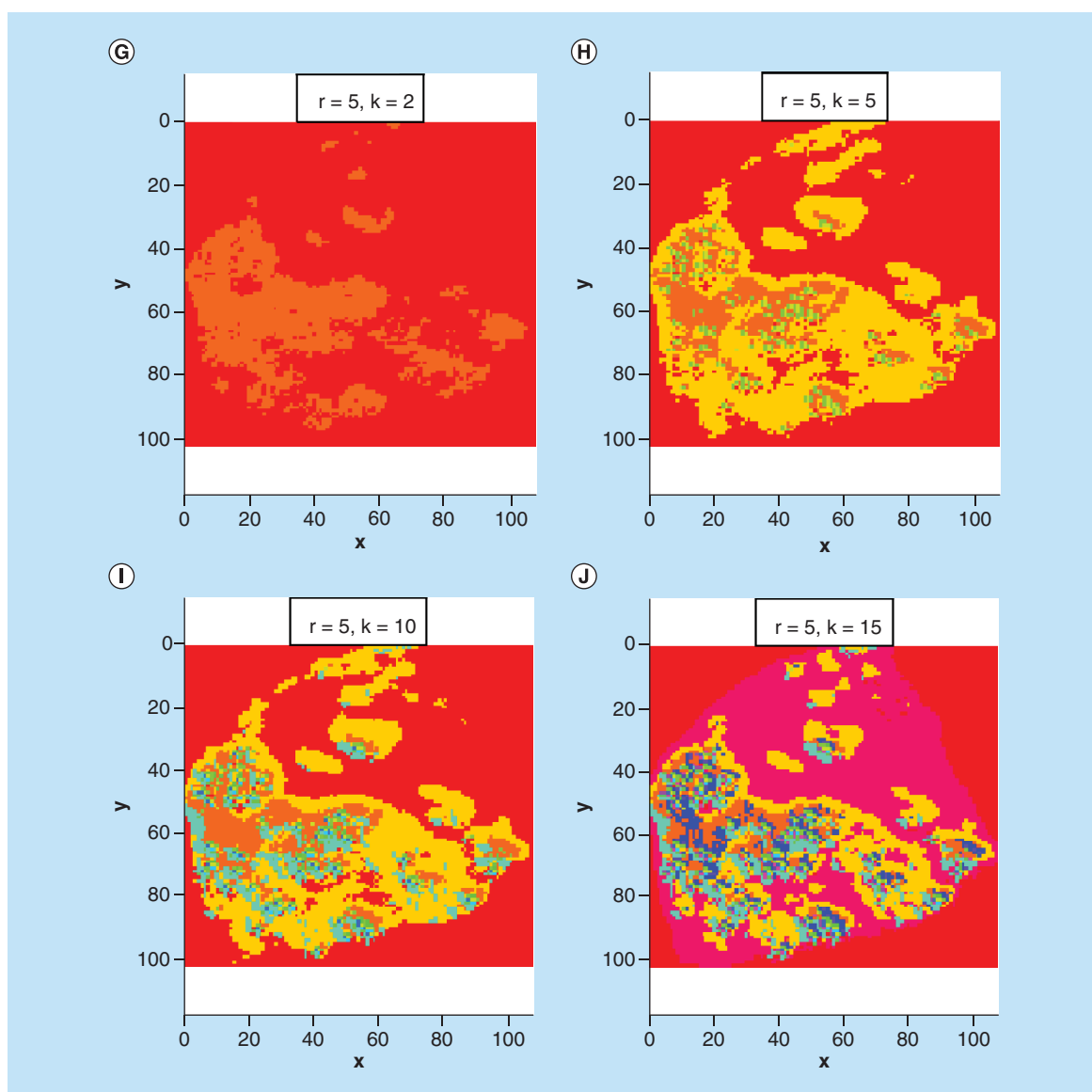


Figure 2. Statistical analysis of MS imaging results (cont.). Graphical representations of spatial distributions for six PCA components generated in Cardinal (A–F) and images of Gaussian k-means clustering of studied imaging data generated with following parameters: smoothing radius $r = 5$, number of segments $k = 2$ (G); $k = 5$ (H); $k = 10$ (I); $k = 15$ (J).

PCA: Principal component analysis.

cancer. The second compound of higher intensity in the healthy tissue region found in form of silver-107 isotope adduct is palmitoyl glucuronide. It is a common liver metabolite of palmitic acid which is excreted by kidneys [41,42]. Similarly to above discussed squalene, higher intensities in normal tissue area are expected. Another compound of higher intensity in the area of normal tissue is *N*-stearoyl arginine also found as ^{107}Ag isotope adduct. The presence of this compound has not been found in human tissues yet, but has been found in the tissues of other mammals. Research results indicate that *N*-stearoyl arginine exhibits antibacterial and antifungal properties [43]. It is worth noting that none of the above chemical compounds has been previously considered as a potential marker for RCC.

Conclusion & future perspective

LDI MSI on AgNPET was performed on surgically removed kidney fragment. Generated ion images showed differences in the spatial distribution of many compounds between healthy tissue and ccRCC areas. Metabolites

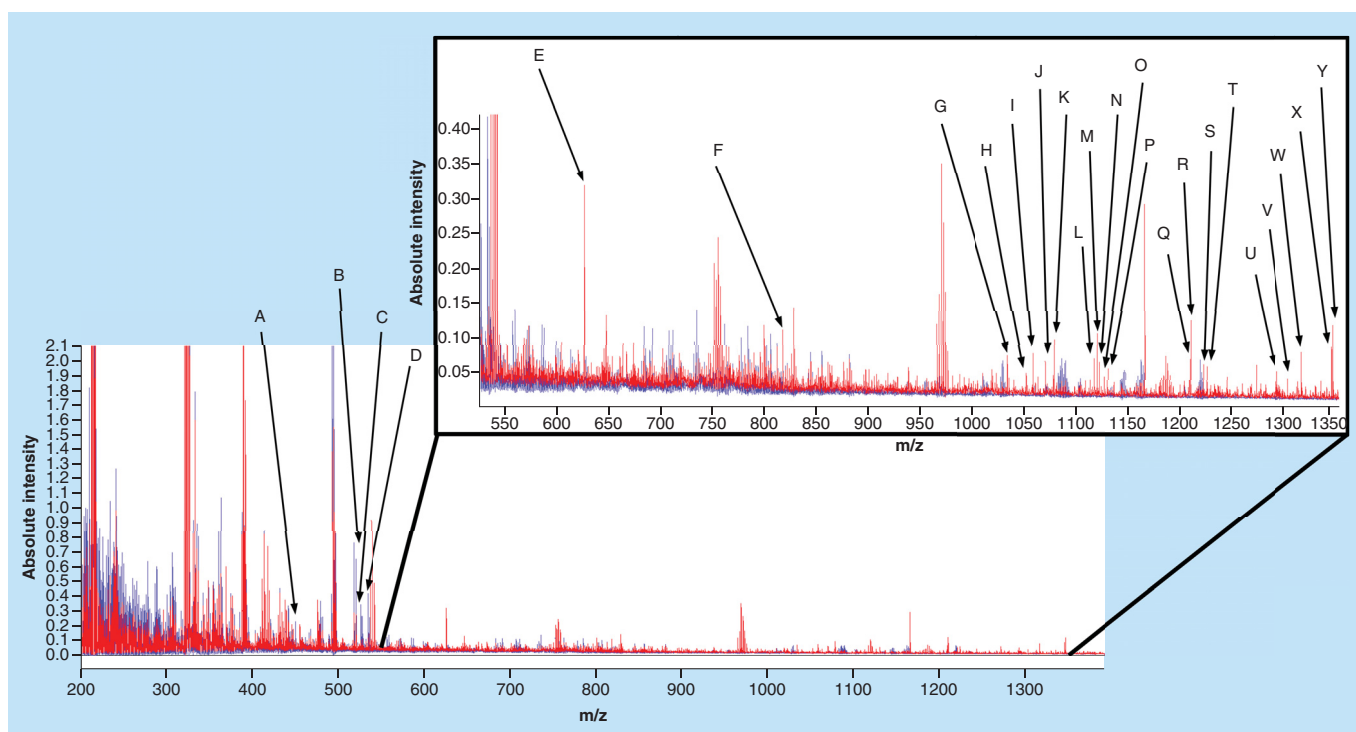


Figure 3. Average spectra for normal (blue line) and cancer (red line) regions.

such as glucose, phenylacetyl glycine, squalene, palmitoyl glucuronide and *N*-stearoyl arginine are mainly located in normal kidney tissue imprint, and sulfinpyrazone sulfide, octadecanamide, arachidonic acid, riboflavin, eicosenoic acid, SAM and *N*-(2-hydroxypentadecanoyl)-4,8-sphingadienine in RCC imprint area. One of listed compounds – octadecanamide was previously pointed out as a potential biomarker in gold nanoparticle-based method [19]. In addition, the comparison of average spectra from the normal and cancer areas revealed a number of *m/z* values for which the intensities in the analyzed normal and cancer areas were distinctly different. Statistical analysis of MSI data with the use of PCA and segmentations allowed the spatial structures to be revealed and compared with the results of pathological examination. The research methodology employed in this work may contribute to the discovery of specific low-molecular-weight biomarkers for RCC, and thus to more effective detection of kidney tumors at early stage of development. In addition, imprint imaging on AgNPET could be used for rapid intraoperative evaluation of the boundary between the tumor and healthy tissue and to confirm the pathologist's assessment.

Supplementary data

To view the supplementary data that accompany this paper please visit the journal website at: www.future-science/doi/suppl/10.4155/bio-2017-0195

Financial & competing interests disclosure

Work funded by National Science Centre (Poland), research project OPUS Number 2016/23/B/ST4/00062. The authors thank German and Polish Bruker-Daltonics for FlexImaging 4.0. Mr Dominik Ruman is acknowledged for creating MS search engine of chemical compounds. The authors have no other relevant affiliations or financial involvement with any organization or entity with a financial interest in or financial conflict with the subject matter or materials discussed in the manuscript apart from those disclosed.

No writing assistance was utilized in the production of this manuscript.

Ethical conduct of research

The authors state that they have obtained the appropriate consent of the local bioethics commission to carry out the research and in addition, for investigations involving human subjects, informed consent has been obtained from the participants involved.

Executive summary

Aim

- One of the most aggressive tumor types is renal cell carcinoma (RCC) that represents 2–3% of all malignant tumors in adults.
- Most of the time, RCC develops asymptotically and a large proportion of patients have metastases at the time of diagnosis which significantly worsens the prognosis.
- For RCC, there are no biomarkers known to date.
- The use of nanoparticle-enhanced target-based laser MS methods can help to discover tumor-specific molecules.

Experimental

- The tumor kidney fragment was obtained from the patient as a result of the surgery.
- Substances from tissue materials were transferred to the silver nanoparticle-enhanced target surface and laser desorption/ionization MS imaging experiments were performed.
- A statistical analysis of the obtained data was made.

Results & discussion

- MS imaging enabled visualization of spatial distributions of nine selected metabolites differentiating between RCC and normal kidney tissue.
- The use of statistical analysis methods such as principal component analysis and spatial segmentation revealed the spatial structures hidden in the set of imaging data that distinguish cancer and healthy tissue without the pathologist's participation.
- The analysis of MS spectra allowed finding another 22 compounds differentiating healthy and RCC areas.

Conclusion

- Imaging of tissue imprint on the silver nanoparticle-enhanced target surface and statistical analysis of the results allowed to visualize the differences between RCC and healthy tissue renal tissue.

References

Papers of special note have been highlighted as: • of interest

1. Ferlay J, Soerjomataram I, Dikshit R *et al.* Cancer incidence and mortality worldwide: sources, methods and major patterns in GLOBOCAN 2012. *Int. J. Cancer* 136, E359–E386 (2015).
2. Chow WH, Dong LM, Devesa SS. Epidemiology and risk factors for kidney cancer. *Nat. Rev. Urol.* 7, 245–257 (2010).
3. Moch H. An overview of renal cell cancer: pathology and genetics. *Semin. Cancer Biol.* 23, 3–9 (2013).
4. Gupta K, Miller JD, Li JZ, Russell MW, Charbonneau C. Epidemiologic and socioeconomic burden of metastatic renal cell carcinoma (mRCC): a literature review. *Cancer Treat. Rev.* 34, 193–205 (2008).
5. Lasseigne BN, Burwell TC, Patil MA, Absher DM, Brooks JD, Myers RM. DNA methylation profiling reveals novel diagnostic biomarkers in renal cell carcinoma. *BMC Medicine* 12, 235 (2014).
6. Ngo TC, Wood CG, Karam JA. Biomarkers of renal cell carcinoma. *Urol. Oncol.* 32, 243–251 (2014).
7. Monteiro MS, Carvalho M, de Lourdes Bastos M, de Pinho PG. Biomarkers in renal cell carcinoma: a metabolomics approach. *Metabolomics* 10, 1210–1222 (2014).
8. Bateson H, Saleem S, Loadman PM, Sutton CW. Use of matrix-assisted laser desorption/ionisation mass spectrometry in cancer research. *J. Pharmacol. Toxicol. Methods* 64, 197–206 (2011).
9. Rodrigo MAM, Zitka O, Krizkova S, Moullick A, Adam V, Kizek R. MALDI-TOF MS as evolving cancer diagnostic tool: a review. *J. Pharm. Biomed. Anal.* 95, 245–255 (2014).
10. Gianazza E, Chinello C, Mainini V *et al.* Alterations of the serum peptidome in renal cell carcinoma discriminating benign and malignant kidney tumors. *J. Proteomics* 76, 125–140 (2012).
11. Schwamborn K, Caprioli RM. Molecular imaging by mass spectrometry – looking beyond classical histology. *Nat. Rev. Cancer* 10, 639–646 (2010).
12. Herring KD, Oppenheimer SR, Caprioli RM. Direct tissue analysis by matrix-assisted laser desorption ionization mass spectrometry: application to kidney biology. *Semin. Nephrol.* 27, 597–608 (2007).
13. Oezdemir RF, Gaisa NT, Lindemann-Docter K *et al.* Proteomic tissue profiling for the improvement of grading of noninvasive papillary urothelial neoplasia. *Clin. Biochem.* 45, 7–11 (2012).
14. Morgan TM, Seeley EH, Fadare O, Caprioli RM, Clark PE. Imaging the clear cell renal cell carcinoma proteome. *J. Urol.* 189, 1097–1103 (2013).
15. Steurer S, Seddiqi AS, Singer JM *et al.* MALDI imaging on tissue microarrays identifies molecular features associated with renal cell cancer phenotype. *Anticancer Res.* 34, 2255–2262 (2014).

16. Na CH, Hong JH, Kim WS *et al.* Identification of protein markers specific for papillary renal cell carcinoma using imaging mass spectrometry. *Mol. Cells* 38, 624–629 (2015).
17. McDonnell LA, Corthals GL, Willems SM, van Remoortere A, van Zeijl RJM, Deelder AM. Peptide and protein imaging mass spectrometry in cancer research. *J. Proteomics* 73, 1921–1944 (2010).
18. Sunner J, Dratz E, Chen YC. Graphite surface-assisted laser desorption/ionization time-of-flight mass spectrometry of peptides and proteins from liquid solutions. *Anal. Chem.* 67, 4335–4342 (1995).
19. Nizioł J, Ossoliński K, Ossoliński T *et al.* Surface-transfer mass spectrometry imaging of renal tissue on gold nano-particle enhanced target. *Anal. Chem.* 88, 7365–7371 (2016).
- **Presents the results of MS imaging of renal cell carcinoma tissue imprint on gold nanoparticles.**
20. Sekula J, Nizioł J, Rode W, Ruman T. Silver nanostructures in laser desorption/ionization mass spectrometry and mass spectrometry imaging. *Analyst* 140, 6195–6209 (2015).
- **Review article on the use of silver nanoparticles in laser desorption/ionization MS.**
21. Nizioł J, Rode W, Zieliński Z, Ruman T. Matrix-free laser desorption–ionization with silver nanoparticle-enhanced steel targets. *Int. J. Mass Spectrom.* 335, 22–32 (2013).
- **Describes the method of preparing silver nanoparticle-enhanced target plates and their use in the analysis of low-molecular-weight compounds.**
22. Bemis KD, Harry A, Eberlin LS *et al.* Cardinal: an R package for statistical analysis of mass spectrometry-based imaging experiments. *Bioinformatics* 31, 2418–2420 (2015).
- **Presents the possibilities and application of Cardinal's package to analyze MS imaging data.**
23. Patiny L, Borel A. ChemCalc: a building block for tomorrow's chemical infrastructure. *J. Chem. Inf. Model.* 53, 1223–1228 (2013).
24. Catchpole G, Platzer A, Weikert C *et al.* Metabolic profiling reveals key metabolic features of renal cell carcinoma. *J. Cell. Mol. Med.* 15, 109–118 (2011).
25. Hirayama A, Kami K, Sugimoto M *et al.* Quantitative metabolome profiling of colon and stomach cancer microenvironment by capillary electrophoresis time-of-flight mass spectrometry. *Cancer Res.* 69, 4918–4925 (2009).
26. Warburg O. On the origin of cancer cells. *Science* 123, 309–314 (1956).
27. Lin L, Huang Z, Gao Y, Yan X, Xing J, Hang W. LC–MS based serum metabolomic analysis for renal cell carcinoma diagnosis, staging, and biomarker discovery. *J. Proteome Res.* 10, 1396–1405 (2011).
28. Lin L, Huang Z, Gao Y *et al.* LC–MS-based serum metabolic profiling for genitourinary cancer classification and cancer type-specific biomarker discovery. *Proteomics* 12, 2238–2246 (2012).
29. Delaney J, Neville WA, Swain A, Miles A, Leonard MS, Waterfield CJ. Phenylacetylglycine a putative biomarker of phospholipidosis: its origins and relevance to phospholipid accumulation using amiodarone treated rats as a model. *Biomarkers* 9, 271–290 (2004).
30. Matsuyama M, Yoshimura R. The target of 5-lipoxygenase is a novel strategy over human urological tumors than the target of cyclooxygenase-2. *Drug Target Insights* 3, 137–151 (2008).
31. Cummings BS. Phospholipase A2 as targets for anti-cancer drugs. *Biochem. Pharmacol.* 74, 949–959 (2007).
32. Higdon J. Riboflavin. Micronutrient Information Center, Linus Pauling Institute, Oregon State University. <http://lpi.oregonstate.edu/mic/vitamins/riboflavin#authors-reviewers>
33. Yang HT, Chao PC, Yin MC. Riboflavin at high doses enhances lung cancer cell proliferation, invasion, and migration. *J. Food Sci.* 78, H343–H349 (2013).
34. Neto AHC, Pelizzaro-Rocha KJ, Fernandes MN, Ferreira-Halder CV. Antitumor activity of irradiated riboflavin on human renal carcinoma cell line 786-O. *Tumor Biol.* 36, 595–604 (2015).
35. Lu SC. S-Adenosylmethionine. *Int. J. Biochem. Cell Biol.* 32, 391–395 (2000).
36. Lu SC, Mato JM. S-Adenosylmethionine in cell growth, apoptosis and liver cancer. *J. Gastroenterol. Hepatol.* 23, S73–S77 (2008).
37. Jones EA, Deininger SO, Hogendoorn PCW, Deelder AM, McDonnell LA. Imaging mass spectrometry statistical analysis. *J. Proteomics* 75, 4962–4989 (2012).
38. Alexandrov T. MALDI imaging mass spectrometry: statistical data analysis and current computational challenges. *BMC Bioinf.* 13, S11 (2012).
39. Edmond J, Fogelman AM, Popjak G. Mevalonate metabolism: role of kidneys. *Science* 193, 154–156 (1976).
40. Newmark HL. Squalene, olive oil, and cancer risk: a review and hypothesis. *Cancer Epidemiol. Biomarkers Prev.* 6, 1101–1103 (1997).
41. Goldstein RS. *Mechanisms of Injury in Renal Disease and Toxicity*. CRC Press FL, USA (1994).
42. Wishart DS, Jewison T, Guo AC *et al.* HMDB 3.0 – the human metabolome database in 2013. *Nucleic Acids Res.* 41, D801–D807 (2013).
43. Tan B, O'Dell DK, Yu YW *et al.* Identification of endogenous acyl amino acids based on a targeted lipidomics approach. *J. Lipid Res.* 51, 112–119 (2010).

